Epigenetic modifications driving ground state pluripotency exit require an NF-κB-independent chromatin IκBα function

Luís G. Palma[1,2,δ], Daniel Álvarez-Villanueva[1,10,δ], María Maqueda[1,2], Mercedes Barrero[7], Arnau Iglesias[1,2], Joan Bertran[9], Damiana Alvarez-Errico[2], Carlos A. García-Prieto[2], Cecilia Ballaré[7], Virginia Rodriguez-Cortez[2], Clara Bueno[2], August Vidal[10], Alberto Villanueva[10], Pablo Menéndez[4,5,11,12,13], Luciano Di Croce[5,7,8], Bernhard Payer[7,8], Manel Esteller[2,4,5,6], Lluís Espinosa[1,*] & Anna Bigas[1,2,*]

[1]Program in Cancer Research. Hospital del Mar Research Institute, CIBERONC, Barcelona, Spain

[2]Josep Carreras Leukemia Research Institute, Barcelona Spain.

[4]Centro de Investigación Biomédica en Red Cancer (CIBERONC), Madrid, Spain.

[5]Institucio Catalana de Recerca i Estudis Avançats (ICREA), Barcelona, Spain.

[6]Physiological Sciences Department, School of Medicine and Health Sciences, University of Barcelona (UB), Barcelona, Catalonia, Spain.

[7]Centre for Genomic Regulation (CRG), The Barcelona Institute of Science and Technology, Barcelona, Spain.

[8]Universitat Pompeu Fabra, Barcelona, Spain.

[9]Faculty of Sciences, Technology and Engineering, Universitat de Vic - Universitat Central de Catalunya, Vic 08500 Spain

[10]Institut Investigació Biomèdica de Bellvitge (IDIBELL), Hospitalet, Barcelona, Spain

[11]Stem Cell Biology, Immunotherapy and Developmental Leukemia Laboratory. Josep Carreras Leukemia Research Institute

[12]Spanish Network for Advanced Therapies (RICORS-TERAV). Carlos III Health Institute (ISCIII).

[13]Department of Biomedicine. University of Barcelona.

[δ] These authors contributed equally

Keywords: IκBα, NFKBIA, NF-κB, DNA Methylation, Polycomb, Embryonic Stem Cells, Pluripotency Exit, Germ Layer Specification,

28 **Corresponding authors:*

29 Anna Bigas and Lluis Espinosa

30 Cancer Research Program. CIBERONC.

31 Hospital del Mar Research Institute

32 Doctor Aiguader 88, 08003, Spain.

33 Tel: +34 933160440; email: abigas@imim.es; lespinosa@imim.es

34

35 **Summary**

36 Inflammatory signals are key in development and cell differentiation but their orchestration
37 with pluripotency and stemness signals is poorly understood. Our previous work identified a
38 chromatin function of IκBα, the NF-κB inhibitor, that is crucial for differentiation in different
39 types of somatic stem cells. Here we demonstrate that deficiency of IκBα imposes a profound
40 chromatin rewiring defect that impacts on DNA methylation, histone post-translational
41 modifications and transcriptional regulation, stabilizing mouse embryonic stem cells (ESCs) in
42 a ground state of pluripotency while preventing them from pluripotency exit and
43 differentiation. By engineering separation-of-function mutants of IκBα with specific binding
44 to either NF-κB or histones, we demonstrate that regulation of pluripotency state by IκBα is
45 independent of NF-κB but requires the chromatin-related IκBα function.

46 **INTRODUCTION**

47 The pluripotent capability of Embryonic Stem Cells (ESCs) allows for the generation of all the
48 somatic and germline lineages both *in vitro* and *in vivo*. However, murine ESCs (mESCs) exhibit
49 high heterogeneity when cultured in serum plus Leukemia Inhibitory Factor (LIF) (S/L
50 medium), with cells interconverting to different metastable states (Festuccia et al. 2013).
51 Some cells retain a ground state pluripotency program, while others are primed for
52 differentiation (Graf and Stadtfeld 2008; Martinez Arias and Brickman 2011). Fluctuations in
53 pluripotency-related transcription factors (Kumar et al. 2014; Filipczyk et al. 2015), microRNA
54 biogenesis (Wang et al. 2007; Kumar et al. 2014) and antagonistic effects on distal regulatory
55 regions (Hu et al. 2022) have been proposed to contribute to this disparity in mESCs. However,
56 the upstream mechanisms governing these interconvertible states remain to be uncovered.

57 The heterogeneity of mESCs can be abolished by culturing the cells with inhibitors of ERK and
58 GS3K signaling, in combination with the use of LIF (2i/L) (Ying et al. 2008). Under both
59 inhibitors plus LIF (2i/LIF) conditions, mESCs enter a ground state of naïve pluripotency
60 promoting homogenous self-renewal while blocking any residual pro-differentiating activity
61 (Ying et al. 2008). Changes in different histone post-translational modifications (PTMs) have
62 been shown to activate pluripotency genes and silence pro-differentiation genes in the
63 ground state (Marks et al. 2012). One of the major epigenetic differences between S/L and
64 2i/L conditions is the global DNA hypomethylation profile observed in mESCs cultured in 2i/L
65 medium (Habibi et al. 2013; Leitch et al. 2013; Singer et al. 2014). However, long-term
66 stabilization of the ground state of pluripotency is detrimental as it can limit the
67 developmental potential of mESCs (Choi et al. 2017). Therefore, identifying novel players to
68 fine-tune the equilibrium between ground and primed states is crucial for preserving both
69 pluripotency stability and differentiation capability in mESCs.

70 Inflammation is an immune response to pathogens that involves different signaling
71 molecules. One of the main effectors of the inflammatory cascade is NF-κB, whose canonical
72 activation involves the phosphorylation of the IKK kinase complex, the phosphorylation and
73 degradation of the NF-κB inhibitor, IκBα, and the nuclear translocation of the NF-κB
74 heterodimer p50/p65 (Zhang, Lenardo, and Baltimore 2017). There is now robust evidence
75 that inflammatory signals are crucial in stem cell development (Gerondakis et al. 2006;
76 Kaltschmidt, Greiner, and Kaltschmidt 2021), though the integration of the inflammatory
77 signals at the pluripotency state is still poorly understood. In this regard, classical NF-κB
78 pathway elements are very lowly expressed in mESCs and overexpression of NF-κB effector
79 proteins leads to loss of pluripotency. In contrast, overexpression of the IκBα super-repressor
80 (S32-36A mutant) has been shown to increase expression of pluripotency markers (Torres and
81 Watt 2008). Similarly, inhibition of Protein Kinase C (PKC) activity in mESCs, which in turn
82 restrains NF-κB signaling, allows keeping mESCs in a ground pluripotency state, thus
83 facilitating the generation of induced pluripotent stem cells (iPSCs) (Dutta et al. 2011).

However, whether NF-κB components affect mESCs function and heterogeneity specifically through regulation of NF-κB signaling or by additional mechanisms remains unknown.

We previously have identified an alternative nuclear function of IκBα involving the interaction with different transcriptional regulators, histone deacetylases (HDACs), core elements of the Polycomb Repressor Complex 2 (PRC2) as well as histones H2A and H4 (Aguilera et al. 2004; Mulero et al. 2013; Marruecos et al. 2021). This nuclear IκBα function is crucial to efficiently silence sets of developmental genes and ensure a proper cell fate specification of somatic stem cells in the epidermis, intestine and hematopoietic stem cells (Mulero et al. 2013; Marruecos et al. 2020, 2021; Thambyrajah et al. 2022). We have now investigated the role of IκBα in the pluripotency of mESCs by using deletion mutants and characterizing their capacity to self-renew and differentiate. We found that lack of IκBα forces a ground chromatin state which involves changes in H3K9me3, H3K4me3 and H3K27me3 levels, and it is coupled with a global DNA hypomethylation in S/L conditions, resembling the ground state of pluripotency. This stabilization of the ground state imposes a block in the pluripotency exit and a general impairment of differentiation. Expression of Separation-of-function (SOF) IκBα mutants that either bind to histones or to NF-κB demonstrate that chromatin-associated IκBα controls heterogeneity in mESCs by an epigenetic rewiring independent of NF-κB function.

RESULTS

IκBα is present in the nucleus of pluripotent embryonic stem cells but not after differentiation

NF-κB-dependent IκBα function takes place mainly in the cytoplasm, whereas chromatin-associated IκBα function occurs in the nucleus (Zhang, Lenardo, and Baltimore 2017). We first investigated IκBα localization in mESCs by immunofluorescence (IF) and western blot (WB). We observed an accumulation of total IκBα in the nucleus and chromatin fractions in pluripotent mESCs (Figures 1A upper panel and 1B). We previously found that nuclear IκBα mainly corresponds to phosphorylated Ser32/36 IκBα (p-IκBα), which is preserved from degradation because of K21 SUMOylation (Mulero et al. 2013). In line with this, our IF analysis showed p-IκBα accumulation in the nucleus of mESCs (Figure 1A bottom panel). In the skin and intestine, nuclear IκBα and p-IκBα are restricted to the stem cell compartments and lost upon differentiation (Mulero et al. 2013; Marruecos et al. 2020). To explore whether a similar distribution happens upon pluripotency exit, we next investigated p-IκBα dynamics in embryoid body (EB) differentiating conditions (Figure 1C upper panel). At 216 hours of culture, most of the cells in EBs were differentiated as detected by the absence of NANOG, and only few cells maintained NANOG expression (Figure 1C bottom panel and 1D). In these conditions, nuclear p-IκBα was restricted to pluripotent cells, co-localizing with NANOG (Figures 1C bottom panel and 1D). These results indicate that p-IκBα is accumulated in the nucleus of pluripotent cells, which is lost upon pluripotency exit. Supporting this observation, RNAseq analysis of mESCs (0h) and early differentiation stages of EBs (48h and 96h), showed that pluripotent cells express higher levels of IκBα gene (*Nfkbia*), which decreases upon differentiation (Figure 1E). Importantly, *Nfkbia* expression follows similar expression dynamics as pluripotency genes (*Dppa4, Zfp42, Prdm14, Klf4, Sox2 and Nanog*), whereas NF-κB members (*Rela, Relb* and *Rel*) and other IκB genes (*Nfkbib*, *Nfkbiz* and *Nfkbie*) showed expression patterns similar to differentiation genes (Figure 1E).

Taken together, these data indicate that p-IκBα protein is specifically present in the nucleus in the pluripotency state of mESCs when *Nfkbia* gene expression is highest.

IκBα is required for pluripotency silencing and the *in vitro* and *in vivo* differentiation of mESCs

To investigate the role of IκBα in pluripotency, we generated IκBα$^{-/-}$ mESC clones by CRISPR-Cas9 with guide RNAs (gRNAs) targeting the first exon of *Nfkbia* (Figure S1A and see Methods section). Initial characterization of three independent IκBα$^{-/-}$ and IκBα$^{+/+}$ mESCs clones demonstrated that lack of IκBα was not affecting expression of the pluripotency marker SSEA-1 (Figure S1B). Cell cycle analysis showed increased number of proliferating cells in IκBα$^{-/-}$ compared to IκBα$^{+/+}$ mESCs (G_2 phase: 15.5%±3.5 in IκBα$^{+/+}$/20.1%±3.5 in IκBα$^{-/-}$; M phase: 2.5%±0.2 in IκBα$^{+/+}$/4.1%±0.7 in IκBα$^{-/-}$) (Figure S1C). Next, we assessed the ability of IκBα$^{-/-}$

138 and IκBα$^{+/+}$ mESCs to differentiate into embryoid bodies (EBs) (Figure S2A) and detected
139 higher numbers of pluripotent cells (NANOG^{+}/OCT3/4^{+}) after 120h of differentiation in IκBα^{-}
140 $^{/-}$ compared to IκBα$^{+/+}$ EBs (Figure S2B). The majority of cells in IκBα$^{-/-}$ EBs maintained a
141 pluripotency state after 216h, when IκBα$^{+/+}$ EBs had only a few small clusters of pluripotent
142 cells remaining (Figure 2A). In addition to the presence of OCT3/4 and NANOG, the higher
143 pluripotency status was confirmed by the presence of Alkaline Phosphatase (AP) assay
144 (Figures 2B and S2C), SSEA-1 (Figures 2C and S2E) as well as the expression of *Pou5f1* (*Oct4*),
145 *Nanog, Zfp42 (Rex1) and Sox2* (Figure S2F). We also observed smaller sizes in EBs from IκBα$^{-/-}$
146 cells (Figure S2D), a feature previously related to lower differentiation potential (Tian et al.
147 2019). To further study the requirement of IκBα in mESC differentiation *in vivo*, we established
148 teratomas by subcutaneous injection of IκBα$^{+/+}$ and IκBα$^{-/-}$ mESCs (Figure S2G) in NSG
149 (NOD.Cg-Prkdc^{scid} Il2rg^{tm1Wjl}/SzJ) mice. IκBα$^{-/-}$ teratomas show a decreased differentiation
150 potential, as indicated by the presence of less differentiated structures (Figure S2H) and the
151 higher number of OCT4^{+} cells (Figures 2D and 2E).

152 The lack of differentiation capability of IκBα$^{-/-}$ mESCs was confirmed at the transcriptomic
153 level by RNAseq of mESCs and EBs at 48h and 96h in differentiation medium (Figure 2F and
154 supplementary table 1). Moreover, IκBα$^{-/-}$ 96h EBs failed to properly silence naïve
155 pluripotency genes (Figures 2G, 2K, S3B-D) while they cannot activate differentiation
156 programs of germ layer (endoderm, mesoderm and ectoderm) specification (Figures 2H-K).
157 These results support the pluripotency fate retention in IκBα$^{-/-}$ mESCs upon differentiation
158 conditions. Notably, we did not detect major changes in the expression levels of NF-κB
159 signaling pathway genes neither at IκBα$^{-/-}$ mESCs nor in IκBα$^{-/-}$ EBs 48h and IκBα$^{-/-}$ EBs 96h
160 (Figure S1D), suggesting that the phenotype imposed by IκBα deficiency is not due to aberrant
161 NF-κB signaling. This could be due to the fact that there is no NF-κB activity in mESCs that
162 need to be repressed by IκBα, or the NF-κB-related IκBα function might be compensated by
163 other IκBs, as previously demonstrated (Hayden and Ghosh 2008).

164 Altogether, our results demonstrate that the lack of IκBα in mESCs imposes a blockade at the
165 pluripotency state which inhibits differentiation in both *in vivo* and *in vitro* conditions without
166 affecting canonical NF-κB signaling.

167 **Absence of IκBα stabilizes the ground state pluripotency through epigenetic rewiring in**
168 **mESCs**

169 *In vitro* cell states for mESCs are highly heterogeneous mimicking different embryonic states
170 and range from a highly pluripotent (ground) state to primed for differentiation (Graf and
171 Stadtfeld 2008; Martinez Arias and Brickman 2011). To investigate the role of IκBα in
172 pluripotency, we performed a Gene Set Enrichment Analysis (GSEA) over IκBα$^{+/+}$ and IκBα$^{-/-}$
173 mESCs comparing gene signatures for ground and primed states of mouse ESC
174 pluripotency(Hu et al. 2022). We found that IκBα$^{-/-}$ mESCs transcriptome is significantly
175 enriched for genes specifically expressed in the ground state, while negatively correlating with

176 the primed state (Figure 3A). These results suggested that IκBα is required for the transition
177 from ground to primed states, which is characterized by an important epigenetic rewiring that
178 involves histone post-translational modifications and DNA methylation. To further investigate
179 the state of IκBα$^{-/-}$ mESCs, we performed genome-wide profiling of H3K4me3, H3K27me3 and
180 H3K9me3 by Chromatin Immunoprecipitation followed by sequencing (ChIP-seq). In general,
181 IκBα$^{-/-}$ mESCs showed a more permissive chromatin status with a predominant enrichment of
182 H3K4me3, loss of H3K9me3 and redistribution of H3K27me3 (Figures 3B, 3C, 3E, 3G, 3I and
183 Figures S3E, S3F, S3H, S3I, and supplementary table 2). Gain of H3K4me3 was found in genes
184 associated to pluripotency such as *Klf2, Zfp42 (Rex1), Sall4* and *Esrrb* (Figures 3C-E and S3E),
185 and it directly correlates with their increased expression in IκBα$^{-/-}$ mESCs (Figure 3F). Analysis
186 of the H3K27me3 mark in IκBα$^{-/-}$ mESCs showed a slight increase of the number of regions
187 with higher H3K27me3 (1070 regions) (Figures 3B, 3G and S3F). Notably, the subset of genes
188 with loss of the H3K27me3 mark (612 regions) were associated with mechanisms of
189 pluripotency (Figure 3H), including those genes associated to the ground state of
190 pluripotency, such as *Tbx3, Klf4* and *Gbx2*, whose transcription is upregulated in IκBα$^{-/-}$ mESCs
191 (Figures 3I and S3G).

192 Analysis of the H3K9me3 mark showed a significant reduction in the detection of regions
193 enriched for this mark in IκBα$^{-/-}$ mESCs (87 regions gained and 450 regions lost) (Figures 3B,
194 S3H, S3I). Among regions with decreased levels of H3K9me3, we found that they mainly
195 correspond to DNA-methylated and imprinted regions (Figures 3J and S3J), which gain
196 H3K4me3 decoration and gene expression (Figures 3J and S3K). H3K9me3 is associated with
197 heterochromatin and DNA methylation (Allis and Jenuwein 2016). We evaluated the DNA
198 methylation levels in IκBα$^{+/+}$ and IκBα$^{-/-}$ mESCs by immunofluorescence. We found a strong
199 decrease in the 5-methylCytosine (5mC) signal in the absence of IκBα (Figure 3K), suggesting
200 a hypomethylation phenotype. To further investigate the specific changes in DNA
201 methylation, we performed a DNA methylation array (Zhou et al. 2022) in IκBα$^{+/+}$ and IκBα$^{-/-}$
202 mESCs and 96h EBs. IκBα$^{-/-}$ mESCs showed a global DNA hypomethylation profile which
203 persists upon induction of differentiation at 96h compared to the IκBα$^{+/+}$ counterparts
204 (Figures 3L, S4A-C). Analysis of differentially methylated regions (DMPs; $\Delta\beta < 0.3$) identified
205 9940 hypomethylated regions specifically in IκBα$^{-/-}$ mESCs, 1497 in IκBα$^{-/-}$ 96h EBs and 518
206 common regions among both timepoints (Figure 3M and supplementary table 3). Specifically,
207 DNA-hypomethylated positions exclusively found in IκBα$^{-/-}$ mESCs correspond to regions of
208 heterochromatin typically decorated by H3K9me2 (Figure S4D). Motif enrichment analysis of
209 IκBα$^{-/-}$ 96h-EBs hypomethylated regions identified target enhancers for pluripotency-related
210 factors such as PRDM14, ESRRB, NANOG (Figure S4E). Moreover, positions that were
211 commonly hypomethylated in mESCs and 96h EBs IκBα$^{-/-}$ corresponded to imprinted regions
212 enriched in H3K9me3 (also confirmed by H3K9me3 ChIP-seq in mESCs (Figure 3J, Figure S3H-
213 J)) and generally bound by the SETDB1/TRIM28 complex (Figure S4F).

214 These results suggest that IκBα in mESCs regulates different chromatin-modifying activities,
215 including histones PTMs and DNA methylation, which specifically affects pluripotency genes.

216 Moreover, our data supports previous studies indicating that long-term stabilization of the
217 ground state of pluripotency limits the developmental potential of mESCs (Choi et al. 2017).

218 **Chromatin function of IκBα induces changes in ground state pluripotency and pluripotency**
219 **exit in an NF-κB independent manner**

220 Uncovering the actual impact of chromatin-related IκBα functions is challenging due to the
221 predominant role of this protein on NF-κB regulation. Recent work from our group has
222 identified the residues in the IκBα protein which are responsible to specifically interact with
223 NF-κB subunits or with histones, and we have generated separation-of-function (SOF) IκBα
224 mutants which retain either NF-κB or chromatin-dependent functions (Álvarez-Villanueva et
225 al. 2023). Taking advantage of IκBα$^{-/-}$ mESCs, we generated different doxycycline-inducible
226 IκBα (i-IκBα) expressing cell lines containing either a wildtype IκBα protein (i-IκBα^{WT}) or one
227 of the SOF IκBα mutants: the one that interacts with NF-κB and it is deficient for H2A/H4
228 binding (IκBα$^{\Delta H2A/H4}$) or the one that interacts with H2A/H4 but not with NF-κB (IκBα$^{\Delta NF\text{-}\kappa B}$)
229 (Figures 4A, S5A). By pull down experiments, we confirmed that IκBα$^{\Delta NF\text{-}\kappa B}$ was able to interact
230 with histone H2A but not with the NF-κB member p50 (Figures S5C and S5D), although in our
231 conditions it can still interact with p65 (Figure S5D). On the other hand, IκBα$^{\Delta H2A/H4}$ can
232 interact with the classical NF-κB heterodimer p50-p65, but it cannot bind H2A (Figures S5C
233 and S5D). As expected, IκBα^{WT} is able to bind to both H2A and NF-κB. To address how IκBα is
234 mediating the stabilization of the ground state in mESCs, we induced expression of i-IκBα^{WT},
235 i-IκBα$^{\Delta NF\text{-}\kappa B}$ and i-IκBα$^{\Delta H2A/H4}$ in IκBα$^{-/-}$ mESCs by overnight (16h) treatment of doxycycline.
236 Temporary induction of i-IκBα^{WT} and i-IκBα$^{\Delta NF\text{-}\kappa B}$ was enough to decrease expression of
237 pluripotency genes *Tbx3, Gbx2, Klf4, Zfp42* and *Nanog*, and to induce differentiation markers
238 (Figures 4B and 4C). Notably, induction of i-IκBα$^{\Delta H2A/H4}$ represses most of the differentiation
239 genes and it causes upregulation of the naïve pluripotency genes *Zfp42* and *Klf2* (Figures 4B
240 and 4C). In addition, the ground state-associated DNA hypomethylation was reverted upon
241 expression of i-IκBα^{WT} and i-IκBα$^{\Delta NF\text{-}\kappa B}$ but not upon i-IκBα$^{\Delta H2A/H4}$ induction (Figure 4D). These
242 results demonstrate that the chromatin-dependent IκBα function, but not its NF-κB-related
243 activity, is necessary and sufficient to revert the ground state of pluripotency with higher DNA
244 methylation levels and lower pluripotency gene expression.

245 In order to address which IκBα activities were required for full mESC differentiation, we
246 induced EB differentiation in i-IκBα^{WT}, i-IκBα$^{\Delta NF\text{-}\kappa B}$ and i-IκBα$^{\Delta H2A/H4}$ lines (Figure S5E).
247 Induction of i-IκBα^{WT} and i-IκBα$^{\Delta NF\text{-}\kappa B}$ in EBs restored the differentiation potential in IκBα$^{-/-}$
248 mESCs (Figures 4E-G and S5E-G). In both conditions, we observed that the number of
249 pluripotent-like cells (NANOG^{+} and OCT3/4^{+}) remaining at 216h EBs was similar to the ones
250 observed at IκBα$^{+/+}$ EBs (Figures 4E, S5F and 2A), and only small and few patches of
251 undifferentiated cells are observed. On the other hand, induction of i-IκBα$^{\Delta H2A/H4}$ did not
252 restore the differentiation potential of IκBα$^{-/-}$ and most of the EB cells were still expressing
253 high levels of NANOG and OCT3/4 at 216h. To further define the differentiation potential of
254 i-IκBα^{WT}, i-IκBα$^{\Delta NF\text{-}\kappa B}$ and i-IκBα$^{\Delta H2A/H4}$ EBs after 216h, we performed AP staining as well as

255 analysis of SSEA-1. We found that expression of i-IκBα^{WT}, i-IκBα$^{\Delta NF\text{-}\kappa B}$ reduced the number of
256 undifferentiated AP^{+} colonies obtained from the EBs (Figure 4F). In agreement with this
257 observation, the number and proportion of cells lacking expression of the pluripotency
258 marker SSEA-1 in the EBs was partially restored upon induction of i-IκBα^{WT} and i-IκBα$^{\Delta NF\text{-}\kappa B}$ but
259 not i-IκBα$^{\Delta H2A/H4}$ (Figures 4G and S5G).

260 Taken together, these results indicate that chromatin-dependent IκBα function controls the
261 balance between ground and primed-to-differentiate states of pluripotency in mESCs in an
262 NF-κB independent manner, and it is required for cells to exit pluripotency and activate the
263 differentiation programs.

264 **DISCUSSION**

265 We here identified a new and unexpected function for the IκBα protein in the regulation of
266 pluripotency and differentiation. Using mESCs to investigate the role of IκBα in differentiation,
267 we discovered that the absence of IκBα severely impairs the exit of pluripotency.
268 Furthermore, IκBα$^{-/-}$ mESCs acquire a ground state of pluripotency, indicating the role of IκBα
269 as a regulator of the transition between ground and primed states. While IκBα is primarily
270 known as an inhibitor of the NF-κB signaling pathway, our lab has previously provided strong
271 evidence of its alternative role by binding to histones and other chromatin elements. We have
272 demonstrated that chromatin-bound IκBα has a crucial role in regulating skin and intestinal
273 stem cells (Mulero et al. 2013; Marruecos et al. 2020), as well as affecting the regenerative
274 capacity of these tissues and the neoplastic transformation. Differentiating this chromatin
275 function of IκBα from its NF-κB inhibitory function has been challenging, making it difficult to
276 determine its significance. To address this, we have engineered separation-of-function (SOF)
277 mutants of IκBα (Álvarez-Villanueva et al. 2023) by identifying specific residues that are
278 essential to bind to NF-κB elements or histones. By reintroducing these mutants into IκBα-
279 deficient mESCs, we have shown that only the histone-binding proficient IκBα mutant
280 (IκBα$^{\Delta NF\text{-}\kappa B}$) with deficient NF-κB binding can restore the differentiation capacity of mESCs.
281 Similarly, we found that the same IκBα$^{\Delta NF\text{-}\kappa B}$ mutant is able to restore differentiation capacity
282 in intestinal cells (Álvarez-Villanueva et al. 2023). The role of NF-κB in mESC differentiation
283 and pluripotency has been previously explored, and while several reports suggest that NF-κB
284 activity correlates with differentiation and loss of pluripotency (Torres and Watt 2008), others
285 claim that NF-κB inhibition correlates with a decrease in pluripotency gene expression
286 (Armstrong et al. 2006). In any case, since modification of canonical NF-κB activity directly
287 impacts on the levels IκBα expression, the previous NF-kB associated phenotypes should be
288 reevaluated considering this chromatin role of IκBα.

289 Our results support the observation that expression of NF-κB elements is low in
290 undifferentiated mESCs and increases with differentiation (Figure 1E). Moreover, the
291 expression of IκBα$^{\Delta H2A/H4}$, which retains the inhibitory function of NF-κB, cannot reconstitute
292 differentiation capacity in cells that lack IκBα (Figures 4 and S5) indicating that the observed
293 IκBα function in controlling pluripotency exit is not due to NF-κB inhibition. In fact, there is
294 evidence that the chromatin function of IκBα is an ancestral function preceding its role as NF-
295 κB inhibitor. In Caenorhabditis elegans (*C.elegans*), which lacks NF-κB orthologs but possesses
296 two IκBα homolog genes, the absence of IκBα orthologs has severe multi-organ
297 differentiation defects (Brena et al. 2020). In mice, IκBα-deficiency results in perinatal death
298 without major developmental defects in the early stages of embryogenesis, which suggest
299 that other mechanisms may compensate for the lack of IκBα *in vivo*. Alternatively, we
300 speculate that in vitro maintenance of pluripotency is differentially regulated compared to
301 blastocyst development.

302 We found that IκBα$^{-/-}$ mESCs exhibit an epigenetic and transcriptomic profile that is
303 compatible with a ground state of pluripotency, strongly suggesting that temporary inhibition
304 of IκBα in mESCs or iPSCs could be used to modulate ground versus primed pluripotency. Our
305 results show that IκBα-deficient mESCs exhibit general DNA hypomethylation, loss of
306 heterochromatin mark H3K9me3 in imprinted genes and a general gain of H3K4me3
307 activation mark (Figure 3). These results suggest IκBα to be a crucial member of a complex
308 which indirectly regulates different histones PTMs and it allows a permissive chromatin status
309 to successfully allow the exit from pluripotency. Nevertheless, the chromatin target regions
310 of IκBα as well as its chromatin partners need to be identified.

311 Additionally, H3K27me3 is modified in several genomic regions, although there is no net gain
312 or loss of this mark. We have previously demonstrated that IκBα interacts with various
313 elements of the Polycomb Repressor Complex 2 (PRC2) in epidermal and intestinal stem cells
314 (Mulero et al. 2013; Marruecos et al. 2020), an interaction that is conserved in *Drosophila*
315 *(Mulero et al. 2013)* and *C.Elegans* (Brena et al. 2020). While we have not observed this
316 physical interaction in mESCs, it is likely that some of these changes result from IκBα
317 modifying the activity of the PRC2 complex.

318 Overall, our work demonstrates that a chromatin activity of IκBα controls pluripotency states
319 in mESCs through an epigenetic rewiring which permits pluripotency exit in an NF-κB-
320 independent manner.

METHODS

Cell lines and culture mediums

HEK293T and NIH/3T3 cell lines were obtained from American Type Culture Collection (ATCC; HEK293T: Cat #CRL-3216; NIH/3T3: Cat #CRL-1658). They were cultured in Dulbecco's modified Eagle's medium (DMEM; Invitrogen Cat #11965092) supplemented with 10% fetal bovine serum (FBS; Biological Industries Cat #04-001-1A), 4.5 g/L glucose (Life Technologies Cat #A2494001), 2 mM L-glutamine (Biological Industries Cat #03-020-1A), 56 U/mL penicillin and 56 µg/mL streptomycin (Biological Industries Cat #03-031-1B).

mESC line ES-E14TG2a (ATCC; Cat #CRL-1821) was cultured on plastic dishes precoated with 0.1% (w/v) Gelatin (Sigma; G2500-100G) with DMEM-ES medium. DMEM-ES is composed by DMEM basal medium (Sigma-Aldrich; Cat #D5796) supplemented with 15% FBS (ESC-qualified; Gibco Cat #26140079), 1X Glutamax (Gibco; Cat #35050061), 1X NEAA (Gibco; Cat#11140050), 1mM Sodium Pyruvate (Gibco; Cat#11360070), 103U/mL Leukemia Inhibitory Factor (LIF) (Millipore, Cat #ESG1107) and 0.125mM 2-mercaptoethanol (Gibco; Cat#31350010).

Medium was changed every day, and cells were splitted every other day using TrypLE Express (Gibco; Cat #12605010) for harvesting. Cells were maintained in a 5% CO2 incubator at 37°C.

Embryoid bodies differentiation from mESCs

Embryoid bodies differentiation was established as described in (Sroczynska et al. 2009). Briefly, mESCs were thawed and passed twice in DMEM-ES before inducing differentiation. After the second passage, and once mESCs are 80% confluent, cells are trypsinized with TrypLE Express. One well of 6-well plate was splitted in an entire 6-well plate in IMDM-ES medium for 48h. IMDM-ES medium is composed of Iscove's Modified Dulbecco's Medium (IMDM) supplemented with 20% FBS (ESC-qualified; Gibco Cat #26140079), 1X Glutamax (Gibco; Cat #35050061), 1X NEAA (Gibco; Cat#11140050), 1mM Sodium Pyruvate (Gibco; Cat#11360070), 10ng/mL Leukemia Inhibitory Factor (LIF) (Millipore, Cat #ESG1107) and 0.125mM 2-mercaptoethanol (Gibco; Cat#31350010).

For embryoid body induction, mESCs were harvested by trypsinization with TrypLE, and they were rinsed twice with 1X PBS to remove any traces of LIF, since this one can inhibit a proper EB differentiation. Cells were very well disaggregated into single-cells, and 1.2 x 104 cells/mL embryoid body differentiation (EBdiff) medium were resuspended to a total volume of 25mL of EBdiff medium. Embryoid body differentiation medium is composed by IMDM supplemented with 15% FBS (ESC-qualified; Gibco Cat #26140079), 1X Glutamax (Gibco; Cat #35050061), 50 µg/mL ascorbic acid (Sigma; Cat #A-4544), 180 µg/mL Transferrin (Roche; Cat #10652202001) and 0.45 mM alpha-monothioglycerol (MTG) (Sigma; Cat #M6145). EBs were formed in suspension for 5 days (120h). At day 5, in order to elongate the differentiation up

357 to 216h (day 9), EBdiff medium was refreshed by harvesting EBs with 10mL serological
358 pipette, centrifuge at 200 g for 3 min and EBs were resuspended in fresh EBdiff medium for 4
359 days longer.

360 **CRISPR/Cas9 gene editing in mESCs**

361 The two guide RNAs (gRNAs) targeting the Nfkbia locus were designed using the CRISPR design
362 tool from MIT (http://crispr.mit.edu.sare.upf.edu). The best 2 gRNAs (based on on-target and
363 off-target scores) that were targeting the exon 1 of Nfkbia (IκBα gene) were selected. After
364 annealing, one of the gRNAs was cloned into SpCas9(BB)-2A-GFP (px458) plasmid (Addgene;
365 Cat #48138), and the other gRNA was cloned into the px330-mCherry plasmid (Addgene; Cat
366 #98750). mESCs were transfected with the two plasmids (px458-gRNA1 and px330-mCherry-
367 gRNA2) at the same time, following the DECKO (Double Excision CRISPR Knockout) approach
368 (Aparicio-Prat et al. 2015). Briefly, $3x10^5$ cells were seeded a day before. At day of
369 transfection, cells were washed once with 1X DPBS (Gibco; Cat #14190144), and Opti-MEM
370 medium (Gibco; Cat #31985070) was added. 1.25 µg of each plasmid (2.5 µg of total DNA)
371 was incubated with 10 µL of Lipofectamine 2000 (Invitrogen; Cat #11668019) in 240 µL of
372 Opti-MEM for 20 min. OptiMEM::Lipofectamine::DNA mixture was added into mESCs, and
373 cells were incubated for 5 hours with the mixture. After that time, cells were washed with
374 PBS, and DMEM-ES was added into the well. 48h after transfection, GFP+ mCherry+ single
375 cells were sorted by FACS using BD FACSAria II Cell Sorter (BD Bioscience). Mutant clones were
376 screened through PCR and western blotting to identify single clones with no IκBα protein
377 expression. Non-targeting scrambled gRNAs were cloned into px458 and px330-mCherry
378 plasmids to generate control clones. Three independent clones from each genotype (wild-
379 type and mutant) were selected for further experiments. gRNAs sequences are included in
380 supplementary table 4.

381 **Teratoma formation assay**

382 IκBα+/+ and IκBα-/- mESCs grown in DMEM-ES (5 × 105) were injected intramuscularly into
383 severe combined immunodeficient mice (NSG). In order to favor 3D aggregation of cells and
384 teratoma formation, cells were resuspended in Matrigel Matrix (BD; Cat #356234) prior to
385 injection. Six weeks later, mice with tumors were euthanized, and tumors were fixed in
386 formaldehyde, embedded in paraffin, sectioned and stained with hematoxylin and eosin for
387 histological analysis.

388 **Immunofluorescence staining**

389 For immunostaining of mESCs, cells were seeded on 0.1% gelatin-coated coverslips on 6-well
390 plates; for EB immunofluorescence, they were collected directly from the plate. Samples were
391 washed twice with 1X PBS, and they were fixed at RT for 10 minutes with 4% PFA (Electron
392 Microscopy Sciences; Cat #15713S). After fixation, samples were washed twice with 1X Tris-
393 buffered saline (TBS; 50 mM Tris-Cl, pH 8) and permeabilized and blocked with 1X TBS

394 supplemented with 1% Triton-X100 (MERCK; Cat #9036-19-5) and 6% FBS (Biological
395 Industries; Cat #04-001-1A) for 2h at 4ºC. Samples were washed twice with 1X TBS
396 supplemented with 6% FBS. Primary antibody incubation was performed in 1X TBS plus 6%
397 FBS and 0.5% Triton-X100 for overnight at 4ºC. The following antibodies were used: phospho
398 (Ser32/36) IκBα (1:250; Cell Signaling; Cat #9246), OCT3/4 (1:250; Santa Cruz; Cat #sc-5279),
399 NANOG (1:250; Novus Biologicals; Cat #NB100-588), BRACHYURY (1:200; Invitrogen; Cat
400 #PA5-78422). Samples were then washed 4 times with 1X TBS, 5 min each washing. Secondary
401 antibody incubation was performed in TBS 1X plus 1% BSA (Sigma-Aldrich; Cat #9048-46-8)
402 for 4 h at RT. The following antibodies were used: Alexa Fluor 488 donkey anti-mouse
403 antibody (1:1000; Invitrogen; Cat #A-21202), Alexa Fluor 647 donkey anti-mouse antibody
404 (1:1000; Invitrogen; Cat #A-31571), Alexa fluor 594 goat anti-mouse antibody (1:1000;
405 Invitrogen; Cat #A-11032), Alexa Fluor 488 donkey anti-rabbit antibody (1:1000; Invitrogen;
406 Cat #A-21206), Alexa Fluor 594 donkey anti-rabbit antibody (1:1000; Life Technologies; Cat
407 #A-21207). Samples were washed three times with 1X TBS for 5 min at RT each rinse. Samples
408 were mounted using DAPI Fluoromount-G (Southern Biotech; Cat #0100-20).

409 **Microscopy and image acquisition**

410 Fluorescence images were acquired using Confocal Leica TCS SP5 (Leica Microsystems), and
411 Leica application software LAS AF (Leica Microsystems) was used to visualize the images.
412 Images of teratoma haematoxylin and eosin and immunohistochemistry stainings were
413 acquired using BX61 Olympus Microscope (Olympus), and PRECiV™ 2D Image and
414 Measurement Software (Olympus) was used to visualize the images. The Image J (version
415 1.15) was used for further analysis (Schneider, Rasband, and Eliceiri 2012).

416 **Cell cycle analysis**

417 mESCs were detached from the plates using TrypLE Express, and they were fixed and
418 permeabilized with a FIX & PERM Cell permeabilization kit (Invitrogen, Cat #GAS004) following
419 manufacturer's instructions. Cells were stained with Alexa Fluor 647 Mouse anti-Ki-67
420 antibody (BD Biosciences, Cat #561126) (1:100), and DAPI (5 µg/ml) (Biotium, Cat #BT-40043).
421 Staining with DAPI was done for 30 min, prior to flow cytometry analysis using a BD LSR II Flow
422 Cytometer (BD Bioscience).

423 **Flow cytometry analysis**

424 Cells were purified based on FACS using BD FACSAria II Cell Sorter (BD Bioscience). Cells were
425 sorted at around 3,500 events/second, and at maximum flow rate of 4 and with a 85 µm
426 nozzle. BD LSRFortessa Cell Analyzer or BD LSR II Flow Cytometer (BD Bioscience) were used
427 for Flow Cytometry Analysis experiments. 5 µg/ml of DAPI (Biotium; Cat #BT-40043) was used
428 as a viability dye. Flow cytometry analysis was performed

429 **RNA isolation, cDNA synthesis and quantitative RT-PCR**

430 Total RNA isolation from cells was performed using the RNeasy Plus Mini Kit (Qiagen; Cat
431 #74136) or RNeasy Micro Kit (Qiagen; Cat #74004) following manufacturer's instructions.
432 Amount of RNA was quantified with Nanodrop (Thermo Fisher; Cat #ND2000CLAPTOP), and
433 2 µg of total RNA was retro-transcribed using Transcriptor First Strand cDNA Synthesis Kit
434 (Roche; Cat #04897030001) following the manufacturer's instructions.

435 Quantitative RT-PCR was performed in triplicates for each sample, and SYBR Green I Master
436 Kit (Roche; Cat #04887352001) was used to carry out the reaction. qRT-PCR reaction was done
437 using the LightCycler 480 system (Roche). Gene expression levels were calculated as $2^{-\Delta CT}$
438 normalized with the average CT of the housekeeping gene Tbp or Gapdh. Primer sequences
439 are found in supplementary table 4.

440 **ChIP-seq experiments**

441 mESCs were cross-linked by incubating them in a cross-link solution (50 mM HEPES pH 8.0, 10
442 mM NaCl, 1 mM EDTA, 0.5 mM EGTA (Egtazic acid)) supplemented with 0.5% formaldehyde
443 (Sigma-Aldrich; Cat #252549). Samples were Incubated for 10 min rocking at RT. Cross-linking
444 was stopped by adding 1.25 M Glycine, 10 mM Tris-HCl pH 8.0 into the sample and incubating
445 for 5 min rocking at RT. Cells were then lysed with 1 mL of lysis buffer (10 mM Tris-HCl pH 8.0,
446 0.25% Triton X-100, 10 mM EDTA, 0.5 mM EGTA, 10 mM Na-butyrate, 20 mM β-glycerol-
447 phosphate, 0.1 mM Naorthovanadate and cOmplete™ Protease Inhibitor Cocktail) for 30 min
448 at 4ºC. Samples were then resuspended in sonication buffer (10 mM Tris-HCl pH 8.0, 0.1 M
449 NaCl, 1 mM EDTA, 0.5 mM EGTA, 10 mM Na-butyrate, 20 mM β-glycerol-phosphate, 0.1 mM
450 Na Orthovanadate and 1% SDS), and they were sonicated using sonication beads (Diagenode;
451 Cat #C01020031) and the Bioruptor Pico Sonicator (Diagenode; Cat #B01060010) for 7 min,
452 to fragment DNA into 500 bp peaces. Fragmented DNA was concentrated using Vivaspin 20
453 columns (Sartorius; Cat #VS2032), and unspecific binding was blocked by incubating the
454 sample with 1% BSA, 1µg salmon sperm DNA, unspecific pre-immune IgG for 2h rocking. To
455 immunoprecipitate, samples were incubated with 5 µg of antibody at 4ºC overnight.
456 Chromatin-IgG complexes were pull down using protein A/G sepharose beads (GE Healthcare;
457 Cat #17-0618-01 and #17-0780-01) for 2h rocking at 4ºC. Cross-linked DNA-protein was
458 reverted by incubating samples at 65 ºC overnight. DNA was purified using GFX Kit (GE
459 Healthcare Life Sciences; Cat #28-9034-71), following the manufacturer's instructions.

460 Purified DNA concentration and integrity were determined using Agilent Bioanalyzer (Agilent
461 Technologies; Cat #G2939BA). Libraries were prepared using standard protocols. Chromatin
462 was sequenced using Illumina HiSeq platform (Illumina, Inc.) (50bp single-end reads). Samples
463 sequencing depth ranged between, per histone mark: (i) H3K4me3: 26M and 27M reads
464 (average 27M reads), (ii) H3K27me3: 62M and 72M reads (average 67M reads) and (iii)
465 H3K9me3: 71M and 89M reads (average 80M reads).

466 **ChIP-seq data analysis**

Quality control was performed on raw data with FASTQC tool. Raw reads were trimmed to remove adapters presence with Trimgalore (v0.6.6) (Krueger et al., 2020). Default parameters were used except for a minimum quality of 15 (Phred score) and an adapter removal stringency of 3bp overlap. For H3K4me3 and H3K27me3 data, trimmed reads were aligned to reference genome with Bowtie2 (v2.4.4) which was executed with default parameters (Langmead & Salzberg, 2012). Required genome index was built with corresponding GRCm38 fasta file retrieved from Ensembl (http://ftp.ensembl.org/pub/release-102/). Multimapped reads and those exhibiting MAPQ < 20 were removed. For H3K9me3 data, trimmed reads were aligned to reference genome (GRCm38 release 102 from Ensembl) with ShortStack (v3.8.5) (Axtell, 2013). Randomly placed multimappers were removed from the mapped reads. For all three histone marks, duplicated reads were marked with SAMtools (v1.15) (Danecek et al., 2021). Drosophila Melanogaster spike-ins, present in H3K27me3, were discarded. NSC and RSC quality metrics were computed with PhantomPeakQualTools (v1.2) (Landt et al., 2012). ENCODE blacklisted regions (mm10 v2) were removed prior to peak calling except for H3K9me3 (Amemiya et al., 2019). BigWig files were individually generated using deepTools (v3.5.1) bamCoverage with -ignoreDuplicates -binSize 10 -smoothLength 30 -effectiveGenomeSize 2308125349 -normalizeUsing RPGC and -extendReads *Fragment_Length* options. (Ramírez et al., 2016). The effective genome size was particularized to a read length of 50bp and directly retrieved from deepTools web site (https://deeptools.readthedocs.io/en/develop/content/feature/effectiveGenomeSize.html). *Fragment_Length* was retrieved from PhantomPeakQualTools results except for H3K9me3 where 150bp value was considered. For H3K9me3 and H3K27me3 data, peak calling was conducted by means of epic2 (v0.0.52) with -effective-genome-fraction 0.8452 -fragment-size *Fragment_Length* options and chromosome sizes only referring to canonical chromosomes (Stovner & Sætrom, 2019). For H3K4me3 narrow profile, MACS2 (v2.2.7.1) was used to identify peaks with -nomodel -extsize *Fragment_Length* -g 2308125349 options (Zhang et al., 2008). For the three histone marks, peaks were called with adjusted p-values (FDR) < 0.05. Peak annotation was performed with ChIPseeker R (v4.2.1) package (v1.34.1) considering a TSS region range between 5000 bp upstream and 100 bp downstream (Yu et al., 2015). Required TxDb object was generated from the Ensembl GRCm38 gtf file retrieved (http://ftp.ensembl.org/pub/release-102/). A consensus peakset was obtained from the three biological replicates per histone mark and condition (WT or KO). For this purpose, findOverlapsOfPeaks function from ChIPpeakAnno R package (v3.32.0) was used with default parameters (L. J. Zhu et al., 2010).

Differential binding analysis (DBA) was conducted with DiffBind (v3.8.4) per histone mark (Stark & Brown, 2011). Default parameters were used except for the summits parameter which was set to 150bp for H3K4me3 and 500bp for H3K27me3 and H3K9me3 in order to consider, for testing, intervals of 300bp and 1000bp respectively. Summit values were selected to have interval widths between the minimum and first quartile peak width values for each histone mark. EdgeR was the statistical method used for all the three analyses.

507 Differentially bound regions (DBRs) between KO and WT samples were called with adjusted
508 p-values (FDR) < 0.05. Identified DBRs with any annotated gene were plotted with
509 EnrichedHeatmap R package (v1.18.1) (Gu et al., 2018). To summarize replicates per
510 condition, normalizeToMatrix function was used based on corresponding BigWig files in w0
511 mean mode in 50bp windows. Tracks visualization were obtained by means of Integrative
512 Genomics Browser (IGV) tool (Robinson et al., 2011).

513 **RNA-seq experiments**

514 Total RNA from three independent clones from mESCs, 48h EBs and 96h EBs was isolated
515 using the RNeasy Plus Mini Kit (Qiagen; Cat #74136) following manufacturer's instructions.
516 Amount of RNA was quantified with Nanodrop (Thermo Fisher; Cat #ND2000CLAPTOP), and
517 RNA integrity was addressed by agarose gel and Agilent Bioanalyzer (Agilent Technologies;
518 Cat #G2939BA). Libraries sequenced using Illumina HiSeq 2500 (Illumina, Inc.) (125bp paired-
519 end reads). Samples sequencing depth ranged between 35M and 52M reads (average 41M
520 reads) per sample.

521 **RNA-seq data analysis**

522 Quality control was performed on raw data with the FASTQC tool (v0.11.9). Raw reads were
523 trimmed to remove adapter presence with Trimgalore (v0.6.6) (Krueger et al., 2020). Default
524 parameters were used except for a minimum quality of 15 (Phred score) and an adapter
525 removal stringency of 3bp overlap. Trimmed reads were aligned to reference the genome
526 with STAR aligner tool (v2.7.8). STAR was executed with default parameters except for the
527 number of allowed mismatches which was set to 1. Required genome index was built with
528 corresponding GRCm38 gtf and fasta files retrieved from Ensembl
529 (http://ftp.ensembl.org/pub/release-102/). Obtained BAM files with uniquely mapped reads
530 were considered for further analysis. Raw gene expression was quantified using
531 featureCounts tool from subRead software (v2.0.1) with exon as feature (Liao et al., 2014).
532 The raw counts matrix was imported into the R Statistical Software environment (v4.2.1) for
533 downstream analysis. Raw expression matrix included 55,487 genes per 18 samples in total.
534 Experimental design considered three timepoints: mouse ESCs, EBs at 48h and EBs at 96h.
535 Each time point included 6 samples distributed in two conditions: 3xWT and 3xKO. Prior to
536 statistical analysis, those genes with less than 10 raw counts across the 6 samples under test
537 were removed. After pre-filtering, 21,843 genes (mESCs), 21,424 genes (EBs 48h) or 21,664
538 genes (EBs 96h) were available for testing. For visualization purposes, counts were normalized
539 by the variance-stabilizing transformation method as implemented in DESeq2 R package (Love
540 et al., 2014) (v1.38.3). Differential expression analysis (DEA) was conducted with DESeq2.
541 Each time point was independently analyzed. Fitted statistical model included sample
542 conditions as covariable with WT as the reference. Obtained log2 fold change values were
543 shrunken with apeglm shrinkage estimator R package (v1.20.0) (A. Zhu et al., 2019). Raw p-
544 values were adjusted for multiple testing using the Benjamini-Hochberg False Discovery Rate

545 (FDR) (Benjamini & Hochberg, 1995). Differentially Expressed Genes (DEGs) between KO and
546 WT samples were called with adjusted p-values (FDR) < 0.05 and absolute shrunken log2 Fold
547 change > 1. Data visualization was performed with the ggplot2 (v3.4.1).

548 **Genome-wide DNA methylation samples preparation**

549 DNA from frozen mESCs pellets was extracted using DNeasy Blood and Tissue Kit (Qiagen
550 GmbH, Hilden, Germany). Purified genomic DNA was quantified with Qubit (Invitrogen,
551 Carlsbad, CA, USA) according to manufacturer's instructions. Infinium Mouse Methylation
552 BeadChip (Illumina, Inc., San Diego, CA, USA) arrays were used to profile DNA methylation
553 genome wide. This platform allows over 285,000 methylation sites per sample to be
554 interrogated at single-nucleotide resolution. The samples were bisulfite converted using EZ
555 DNA Methylation-Gold™ Kit (Zymo Research, CA, USA) and were hybridized in the array
556 following the manufacturer's instructions.

557 **DNA methylation data analysis**

558 The DNA methylation profile of the studied samples was assessed using the Infinium Mouse
559 Methylation BeadChip Array (~285,000 methylation sites) as previously described (Garcia-
560 Prieto et al., 2022). Briefly, raw signal intensities were obtained with GenomeStudio Software
561 2011.1 (Illumina) and DNA methylation beta values were computed from raw IDAT files using
562 GenomeStudio default normalization with control probes and background subtraction.
563 Quality control steps to remove erratic probe signals were performed within the R statistical
564 environment (v4.0.3). We removed probes with detection p value > 0.01, genotyping probes
565 and manufacturing flagged (MFG) probes described in the Illumina manifest file
566 (https://support.illumina.com/downloads/infinium-mouse-methylation-manifest-file.html).
567 The differentially methylated probes (DMPs) between WT and KO samples were computed
568 separately for each time point (mESCs and EBs at 96h) by deriving a linear model with the
569 limma R package (v3.46.0). Each condition included 3 samples per time point. DMPs with
570 adjusted p-value (FDR) <0.05 and absolute mean methylation beta value difference between
571 conditions >0.3 were considered significant. DNA methylation analysis was performed using
572 the mm10 mouse genome reference build and the complete annotation was downloaded
573 from the annotated manifest file (http://zwdzwd.github.io/InfiniumAnnotation#mouse)
574 (Zhou et al., 2022).

575 **Functional analysis**

576 Overrepresentation analysis was applied over lists of selected genes derived from RNA-seq
577 data (DEGs) or from ChIP-seq data (differentially bound regions). The Gene Ontology
578 (Biological Process ontology, GO BP terms), KEGG PATHWAY and WikiPathways databases for
579 Mus Musculus (Ashburner et al., 2000; Kanehisa & Goto, 2000; Martens et al., 2021) were
580 interrogated by means of clusterProfiler R package (v4.6.2) (Wu et al., 2021). Corresponding
581 Entrez identifiers were used. Benjamini-Hochberg procedure was used to obtain adjusted p-

582 values. Obtained GO BP terms were simplified using the simplify function from clusterProfiler
583 with default parameters. Overrepresented terms or processes were called with adjusted p-
584 values (FDR) < 0.05.

585 Gene Set Enrichment Analysis (GSEA) was performed for mESCs against the three cell states
586 signatures defined by other authors (Hu et al., 2022). Briefly, each signature was composed
587 of 200 genes uniquely expressed in each state obtained from bulk RNA-seq performed per
588 state. For this purpose, the complete list of genes from mESCs samples (21,843 genes) was
589 ranked based on the shrunken log2 Fold Change obtained from DEA. GSEA was conducted
590 thru fgseaMultilevel function from fgsea R package (v1.24.0) (Korotkevich et al., 2021) with
591 default parameters. Enrichment plots were generated with the same package.

592 Additionally, the testEnrichment function from SeSAMe R package (v1.14.2) (Zhou et al.,
593 2018) was used for conducting functional analysis with default parameters over the list of
594 DMPs. Probe design, transcription factor binding site and histone modifications consensus
595 database sets, included in the same package, were interrogated.

596 Gene Set Variation Analysis (GSVA) R package (v1.46.0) with default parameters were used to
597 obtain Z-score values for a particular gene set (Hänzelmann et al., 2013).

DATA AVAILABILITY

All sequencing data is deposited at GEO under a superseries (accession number GSEXXXXX). Individual datasets can be found at: GSEXXXX (RNA-seq data), GSEXXX (ChIP-seq data) and GSEXXX (Methylation array data).

ACKNOWLEDGEMENTS

L.G.P has been a recipient of FI AGAUR fellowship (2019 FI-B 00151/2020 FI_B1 00130) from Generalitat de Catalunya. D.A-V was funded by the FIS fellowship (FI20/00130) from Instituto Carlos III. This work has been supported by Spanish Ministry of Science and Innovation (PID2019-104695RB-I00, PLEC2021-007518, PDC2021-120817-I00), Generalitat de Catalunya (2021SGR 39) and Departament de Salut (SLT002/16/00299) to AB; the Spanish Ministry of Science and Innovation (PID2019-108322GB-100 and PID2022-142679NB-I00) to LDC; the Spanish Ministry of Science and Innovation (PID2021-123383NB-I00.) and the Agencia de Gestió d'Ajuts Universitaris i de Recerca (2021 SGR 01222) to BP. M.B. received funding from the Ramón Areces Foundation. M.M. is a recipient of a grant from the Instituto Carlos III, grant number CA22/00011 (cofunded by the European Social Fund Plus, ESF+ and by the European Union).

AUTHOR CONTRIBUTION

L.G.P, L.E and A.B designed the study. L.G.P, D.A-V, M.B, A.I, J.G, J.B, D.A.E, C.A.G.P, C.B, V.R.C and A.V performed experiments. L.G, M.M and M.B performed bioinformatics analysis. L.G and A.B wrote the manuscript with input from all authors. C.B, A.V, A.V, P.M, L.D.C, B.P, M.E and L.E provided input on experimental design. L.E and A.B provided resources and supervised the research.

621 **FIGURE LEGENDS**

622 **Figure 1. p-IκBα specifically accumulates in the nucleus of pluripotent cells. A.**
623 Immunofluorescence of mESCs stained for total IκBα and OCT3/4 (upper panel), and
624 phosphorylated Se 32/36 IκBα (p-IκBα) co-stained with NANOG (bottom panel). **B.** Western
625 blot analysis of cytoplasm (Cyt), nucleus (Nuc) and chromatin (Chr) from mESCs. Red arrow:
626 specific band for total IκBα. *: non-specific band. **C.** Schematic of EBs differentiation protocol
627 (upper panel). Representative image of immunofluorescence for NANOG and p-IκBα on 216h
628 EBs (lower panel). **D.** Percentage of cells displaying p-IκBα and NANOG protein expression at
629 216h EBs. Each dot represents the average quantification of % cells in five EBs in each
630 independent experiment. **E.** Heatmap representing the normalized and scaled expression of
631 genes related to pluripotency, differentiation and NF-κB pathways at mESCs, 48h embryoid
632 bodies (EBs) and 96h EBs. Three independent IκBα$^{+/+}$ clones are analyzed.

633 **Figure 2. Lack of IκBα prevents pluripotency exit upon induction of *in vitro* and *in vivo***
634 **differentiation.** Representative image of immunofluorescence of 216h EBs stained for
635 NANOG and OCT3/4 from IκBα$^{+/+}$ (upper panel) and IκBα$^{-/-}$ (lower panel) cells. **B.**
636 Quantification of total number of alkaline phosphatase (AP) colonies after 216h EB
637 differentiation and additional culture of 96h in S/L medium. Dots represent independent
638 experiments from three different IκBα$^{+/+}$ or IκBα$^{-/-}$ clones **C.** Percentage of SSEA-1 cells at EBs
639 216h analyzed by flow cytometry. Each dot represents an independent clone. **D.**
640 Representative images of immunohistochemistry for OCT3/4 in IκBα$^{+/+}$ (left panel) or IκBα$^{-/-}$
641 (right panel) teratomas. Teratomas were derived from three independent clones of mESCs of
642 both genotypes. **E.** Percentage of OCT3/4^{+} cells in teratomas. Positive cells were counted by
643 from five different microscope fields from each IκBα$^{+/+}$ and IκBα$^{-/-}$ clone. **F.** Principal
644 component analysis (PCA) based on normalized RNA-seq data from 3 different time points
645 (mESCs, 48h EBs and 96h EBs) of IκBα$^{+/+}$ and IκBα$^{-/-}$ cells. **G, H, I, J.** Z-score from normalized
646 counts retrieved from mESCs, 48h and 96h EBs IκBα$^{+/+}$ or IκBα$^{-/-}$ cells. Pluripotency score (G)
647 refers to the subset of genes from WikiPathways database ('Mechanisms associated with
648 pluripotency' , WP1763) which are differentially expressed at 96h EBs. Genes from the
649 Endoderm (H), Mesoderm (I) and Ectoderm (J) scores are retrieved from corresponding Gene
650 Ontology BP formation terms (GO:0001706, GO:0001707 or GO:0001705, respectively). **K.**
651 Network of selected overrepresented biological pathways (adjusted p-val <0.05, FDR) from
652 WikiPathways database. Pathways are connected through their annotated differentially
653 expressed genes (DEGs) in IκBα$^{+/+}$ vs IκBα$^{-/-}$ comparison at 96h EBs. Pathway circle size is
654 proportional to the number of annotated genes. Gene node color represents shrunken Log_2
655 Fold-change obtained in differential expression analysis.

656 **Figure 3. IκBα controls ground state pluripotency exit through epigenetic rewiring. A.** GSEA
657 results from IκBα$^{-/-}$ vs IκBα$^{+/+}$ mESCs samples against ground and primed state pluripotency
658 signatures retrieved from Hu et al., 2022. **B.** Number of differentially binded regions (adjusted
659 p-val <0.05, FDR) for H3K9me3 (K9me3), H3K4me3 (K4me3) and H3K27me3 (K27me3) histone

660 marks in IκBα $^{-/-}$ compared to IκBα $^{+/+}$ mESCs. Gained or lost regions in IκBα $^{-/-}$ samples are
661 distinguished (log_2 Fold-change >0 or <0, respectively) . **C.** Heatmap of differentially gained
662 and lost H3K4me3 regions in IκBα$^{-/-}$ and IκBα$^{+/+}$ mESCs (adjusted p-val < 0.05, FDR). Only those
663 regions with any associated gene are considered. Highlighted genes are annotated to
664 'Mechanisms associated to pluripotency' pathway from WikiPathways database (WP1763).
665 Regions are sorted per their adjusted p-value obtained from differential binding analysis
666 (DBA). Heatmaps are centered in the region center and extended 3Kb upstream and
667 downstream. Fold Change values are retrieved from DBA. **D.** Functional overrepresentation
668 analysis results of those genes with differential gain of H3K4me3 mark in IκBα$^{-/-}$ mESCs using
669 WikiPathways database. **E.** Tracks showing H3K4me3 distribution for ground state
670 pluripotency genes associated to differential regions in IκBα$^{-/-}$ compared to IκBα $^{+/+}$ mESCs.
671 Shadowed regions highlight the differential levels of the H3K4me3. **F.** Expression analysis
672 (qPCR) of those genes shown in previous panel. **G.** Heatmap of differentially gained and lost
673 H3K27me3 regions in IκBα$^{-/-}$ and IκBα$^{+/+}$ mESCs (adjusted p-val < 0.05, FDR). Only those
674 regions with any associated gene are considered. Highlighted genes are annotated to
675 'Mechanisms associated to pluripotency' pathway from WikiPathways database (WP1763).
676 Regions are sorted per their adjusted p-value obtained from differential binding analysis
677 (DBA). Heatmaps are centered in the region center and extended +/- 3kb. Fold Changes values
678 are retrieved from DBA. **H.** Functional overrepresentation analysis results of those genes with
679 differential lost H3K27me3 mark in IκBα$^{-/-}$ mESCs against WikiPathways database. **I.** Tracks
680 showing H3K27me3 distribution for ground state pluripotency genes associated with
681 differential regions in IκBα$^{-/-}$ mESCs compared to IκBα $^{+/+}$ mESCs. Shadowed regions highlight
682 the differential levels of the H3K27me3. **J.** Tracks showing H3K9me3 and H3K4me3
683 distribution for imprinted genes associated to differential regions in IκBα$^{-/-}$ mESCs compared
684 to IκBα $^{+/+}$ mESCs. Shadowed regions highlight the differential levels of the H3K9me3. **K.**
685 Immunofluorescence of DNA methylation (5mC) in IκBα$^{+/+}$ mESCs (upper) and IκBα$^{-/-}$ (lower)
686 mESCs. **N.** DNA methylation profile in IκBα$^{+/+}$ and IκBα$^{-/-}$ mESCs showing the distribution
687 density of all 261,220 CpGs under test from mean ß-values per condition. **M.** Venn diagram
688 representing differentially DNA hypomethylated regions in either IκBα$^{-/-}$ mESCs or 96h EBs.

689 **Figure 4. Chromatin-associated IκBα controls pluripotency exit in an NF-κB-independent**
690 **manner. A.** Schematic of chromatin-specific/NF-κB-deficient (IκBα$^{\Delta NF\text{-}\kappa B}$) or NF-κB-
691 specific/chromatin-deficient (IκBα$^{\Delta H2A/H4}$) IκBα mutant functions. **B.** Expression analysis of
692 pluripotency markers after inducing IκBα^{WT}, IκBα$^{\Delta NF\text{-}\kappa B}$ and IκBα$^{\Delta H2A/H4}$ in IκBα$^{-/-}$ mESCs. Each
693 dot represents an independent experiment. **C.** Expression analysis of differentiation markers
694 after inducing IκBα^{WT}, IκBα$^{\Delta NF\text{-}\kappa B}$ and IκBα$^{\Delta H2A/H4}$. Each dot represents an independent
695 experiment. **D.** Immunofluorescence of DNA methylation (measured by 5mC) after re-
696 expressing IκBα^{WT}, IκBα$^{\Delta NF\text{-}\kappa B}$ and IκBα$^{\Delta H2A/H4}$ **E.** Immunofluorescence for NANOG and OCT3/4
697 at EBs 216h after induction of IκBα^{WT}, IκBα$^{\Delta NF\text{-}\kappa B}$ and IκBα$^{\Delta H2A/H4}$. **F.** Alkaline phosphatase
698 staining (upper) and quantification (lower) of reconstitution experiments. **G.** Flow cytometry

699 analysis of the pluripotency surface marker SSEA-1 at 216h EBs after IκBα^{WT}, IκBα$^{\Delta NF\text{-}\kappa B}$ and
700 IκBα$^{\Delta H2A/H4}$ induction.

701 **Figure S1. Depletion of IκBα does not compromise neither pluripotency self-renewal nor**
702 **NF-κB activity. A. Upper panel.** Strategy to delete IκBα gene in mESCs using CRISPR/Cas9.
703 Three independent clones from each genotype (IκBα $^{+/+}$ or IκBα$^{-/-}$) were chosen for further
704 experiments. **Lower panel.** Western Blotting for IκBα between IκBα$^{+/+}$ and IκBα$^{-/-}$ clones. **B.**
705 Flow cytometry for the pluripotent surface marker SSEA-1 in IκBα$^{+/+}$ and IκBα$^{-/-}$ mESCs
706 cultured in S/L medium. **C. i)** Representative plots of the cell cycle profile in IκBα$^{+/+}$ and IκBα^{-}
707 $^{/-}$ mESCs by flow cytometry. **ii)** Quantification of cell cycle distribution in three independent
708 mESCs clones from each genotype. **D.** Boxplots and violin plots representing the normalized
709 gene expression levels in IκBα$^{+/+}$ or IκBα$^{-/-}$ mESCs, EBs 48h and EBs 96h. Considered genes are
710 those annotated to NF-κB signaling pathway (KEGG PATHWAY mmu04064). Box Plots: center
711 line, median; box limits, first and third quartiles; whiskers, 1.5× interquartile; points, outliers.
712 Violin plots show the corresponding probability density function. Two-sided Wilcoxon test
713 applied.

714 **Figure S2. Absence of IκBα blocks pluripotency exit upon EB and teratoma formation. A.**
715 Schematic of EB differentiation with brightfield images of different time points of
716 differentiation. **B.** Representative immunofluorescence images of 120h EBs stained for
717 NANOG and OCT3/4 from IκBα$^{+/+}$ (upper panel) and IκBα$^{-/-}$ (bottom panel) cells. **C. i**) Schematic
718 of AP staining experiment. **ii)** Brightfield images from AP colonies from three independent
719 clones from IκBα$^{+/+}$ or IκBα$^{-/-}$. **D.** Quantification of relative size of 168h EBs. Each dot
720 represents one EB. **E.** Flow cytometry plots of SSEA-1 from IκBα$^{+/+}$ or IκBα$^{-/-}$ EBs 96h. **F.**
721 Expression dynamics of different pluripotency markers *Pou5f1 (Oct4), Zfp42, Nanog* and *Sox2*
722 measured across EB differentiation. RNA expression levels were relative to time point 0
723 (mESCs). **G.** Schematic of the protocol to induce teratoma formation in NSG mice. **H.**
724 Hematoxylin & Eosin staining representative images from teratomas formed from
725 independent clones of IκBα$^{+/+}$ or IκBα$^{-/-}$ mESCs. Asterisks denote the presence of immature
726 structures.

727 **Figure S3. Transcriptomic and epigenetic differences in IκBα$^{+/+}$ or IκBα$^{-/-}$ mESCs. A, B, C.**
728 Volcano plots from IκBα$^{-/-}$ against IκBα$^{+/+}$ mESCs (A), 48h EBs (B) and 96h EBs (C) differential
729 expression analysis. Dashed vertical lines represent an absolute shrunkend log2 Fold Change
730 = 1 and dashed horizontal lines represented and adjusted p-value = 0.05 (FDR) **D.** Heatmap of
731 96h EBs in which normalized counts (z-score) of pluripotency or differentiation (gastrulation-
732 related) genes are represented. **E.** Volcano plot of H3K4me3 in IκBα$^{+/+}$ vs IκBα$^{-/-}$ mESCs
733 differential binding analysis. Representative genes with increased levels of H3K4me3 in IκBα^{-}
734 $^{/-}$ mESCs are highlighted. **F.** Volcano plot of H3K27me3 in IκBα$^{+/+}$ vs IκBα$^{-/-}$ mESCs differential
735 binding analysis. Representative genes with decreased levels of H3K27me3 in IκBα$^{-/-}$ mESCs
736 are highlighted. **G.** qPCR analysis of pluripotency genes with decreased levels of H3K27me3
737 in IκBα$^{-/-}$ mESCs. Expression analysis was performed in mESCs. **H.** Heatmap of differentially

738 gained and lost H3K9me3 regions in IκBα$^{-/-}$ and IκBα$^{+/+}$ mESCs (adjusted p-val < 0.05, FDR).
739 Only those regions with any associated gene are considered. Highlighted genes are imprinted
740 genes. Regions are sorted per their adjusted p-value obtained from differential binding
741 analysis (DBA). Heatmaps are centered in the region center and extended +/- 3kb. Fold
742 Change values are retrieved from DBA. **I.** Volcano plot of H3K9me3 in IκBα$^{+/+}$ vs IκBα$^{-/-}$ mESCs
743 differential binding analysis. Representative imprinted genes with decreased levels of
744 H3K9me3 in IκBα$^{-/-}$ mESCs are highlighted. **J.** Functional overrepresentation analysis results of
745 those genes with differential gain of H3K9me3 mark in IκBα$^{-/-}$ mESCs against GO Biological
746 Processes database. **K.** qPCR analysis of imprinted genes with differential loss of H3K9me3 in
747 mESCs.

748 **Figure S4. IκBα$^{-/-}$ mESCs and 96h EBs display a global DNA hypomethylation status. A, B.**
749 DNA methylation levels (mean ß-values) across chromosomes in mESCs (A) or 96h EBs (B). **C.**
750 DNA methylation levels in different genomic regions: promoters, gene bodies, enhancers and
751 imprinted regions (Unpaired T-Test). **D, E, F.** Functional analysis of differentially methylated
752 regions exclusively found in IκBα$^{-/-}$ mESCs (D), 96h EBs (E) or common between time points
753 (F).

754 **Figure S5. Generation of separation-of-function (SOF) IκBα mutants to study how**
755 **chromatin-related IκBα controls pluripotency exit. A.** IκBα$^{-/-}$ mESCs after overnight induction
756 (1µg/mL doxycycline) of the different SOF IκBα mutants. **B.** Quantification of *Nfkbia* mRNA
757 activation upon doxycycline induction in reconstituted IκBα$^{-/-}$ mESCs. **C.** Pull-down of GST-H2A
758 with cell lysates from different SOF IκBα mutant mESCs. **D.** Pull-down of GST-p65 (left) or GST-
759 p50 (right) with lysates from SOF IκBα mutant mESCs. **E.** Western blot analysis of IκBα protein
760 during EB differentiation after 48h of induction. **F.** Quantification of EB differentiation status
761 (percentage of pluripotent cells) at 216h after induction of SOF IκBα mutants. Data from two
762 independent experiments. **G.** Percentage of differentiated cells (determined as SSEA-1
763 negative) at EBs 216h after SOF IκBα induction.

764 **REFERENCES**

765 Aguilera, Cristina, Ruben Hoya-Arias, Guy Haegeman, Lluís Espinosa, and Anna Bigas. 2004.
766 "Recruitment of IκBα to the *hes1* Promoter Is Associated with Transcriptional
767 Repression." *Proceedings of the National Academy of Sciences* 101 (47): 16537–42.
768 Allis, C. David, and Thomas Jenuwein. 2016. "The Molecular Hallmarks of Epigenetic
769 Control." *Nature Reviews. Genetics* 17 (8): 487–500.
770 Álvarez-Villanueva, Daniel, Luis Galán-Palma, Joan Bertran, Martin Floor, Laura Solé, Teresa
771 Lobo-Jarne, María Maqueda, et al. 2023. "Separation-of-Function Mutants Reveal the
772 NF-κB-Independent Involvement of IκBα in the Regulation of Stem Cell and Oncogenic
773 Programs." *bioRxiv*. https://doi.org/10.1101/2023.06.21.545928.
774 Aparicio-Prat, Estel, Carme Arnan, Ilaria Sala, Núria Bosch, Roderic Guigó, and Rory Johnson.
775 2015. "DECKO: Single-Oligo, Dual-CRISPR Deletion of Genomic Elements Including Long
776 Non-Coding RNAs." *BMC Genomics* 16 (October): 846.
777 Armstrong, Lyle, Owen Hughes, Sun Yung, Louise Hyslop, Rebecca Stewart, Ilka Wappler,
778 Heiko Peters, et al. 2006. "The Role of PI3K/AKT, MAPK/ERK and NFkappabeta
779 Signalling in the Maintenance of Human Embryonic Stem Cell Pluripotency and Viability
780 Highlighted by Transcriptional Profiling and Functional Analysis." *Human Molecular*
781 *Genetics* 15 (11): 1894–1913.
782 Brena, David, Joan Bertran, Montserrat Porta-de-la-Riva, Yolanda Guillén, Eric Cornes,
783 Dmytro Kukhtar, Lluís Campos-Vicens, et al. 2020. "Ancestral Function of Inhibitors-of-
784 kappaB Regulates Caenorhabditis Elegans Development." *Scientific Reports* 10 (1):
785 16153.
786 Choi, Jiho, Aaron J. Huebner, Kendell Clement, Ryan M. Walsh, Andrej Savol, Kaixuan Lin,
787 Hongcang Gu, et al. 2017. "Prolonged Mek1/2 Suppression Impairs the Developmental
788 Potential of Embryonic Stem Cells." *Nature* 548 (7666): 219–23.
789 Dutta, Debasree, Soma Ray, Pratik Home, Melissa Larson, Michael W. Wolfe, and Soumen
790 Paul. 2011. "Self-Renewal versus Lineage Commitment of Embryonic Stem Cells:
791 Protein Kinase C Signaling Shifts the Balance." *Stem Cells* 29 (4): 618–28.
792 Festuccia, Nicola, Rodrigo Osorno, Valerie Wilson, and Ian Chambers. 2013. "The Role of
793 Pluripotency Gene Regulatory Network Components in Mediating Transitions between
794 Pluripotent Cell States." *Current Opinion in Genetics & Development* 23 (5): 504–11.
795 Filipczyk, Adam, Carsten Marr, Simon Hastreiter, Justin Feigelman, Michael Schwarzfischer,
796 Philipp S. Hoppe, Dirk Loeffler, et al. 2015. "Network Plasticity of Pluripotency
797 Transcription Factors in Embryonic Stem Cells." *Nature Cell Biology* 17 (10): 1235–46.
798 Gerondakis, S., R. Grumont, R. Gugasyan, L. Wong, I. Isomura, W. Ho, and A. Banerjee. 2006.
799 "Unravelling the Complexities of the NF-kappaB Signalling Pathway Using Mouse
800 Knockout and Transgenic Models." *Oncogene* 25 (51): 6781–99.
801 Graf, Thomas, and Matthias Stadtfeld. 2008. "Heterogeneity of Embryonic and Adult Stem
802 Cells." *Cell Stem Cell* 3 (5): 480–83.
803 Habibi, Ehsan, Arie B. Brinkman, Julia Arand, Leonie I. Kroeze, Hindrik H. D. Kerstens,
804 Filomena Matarese, Konstantin Lepikhov, et al. 2013. "Whole-Genome Bisulfite
805 Sequencing of Two Distinct Interconvertible DNA Methylomes of Mouse Embryonic
806 Stem Cells." *Cell Stem Cell* 13 (3): 360–69.
807 Hayden, Matthew S., and Sankar Ghosh. 2008. "Shared Principles in NF-kappaB Signaling."
808 *Cell* 132 (3): 344–62.
809 Hu, Sofia, Emily Metcalf, Dig Bijay Mahat, Lynette Chan, Noor Sohal, Meenakshi

Chakraborty, Maxwell Hamilton, et al. 2022. “Transcription Factor Antagonism Regulates Heterogeneity in Embryonic Stem Cell States.” *Molecular Cell* 82 (23): 4410–27.e12.

Kaltschmidt, Christian, Johannes F. W. Greiner, and Barbara Kaltschmidt. 2021. “The Transcription Factor NF-κB in Stem Cells and Development.” *Cells* 10 (8). https://doi.org/10.3390/cells10082042.

Kumar, Roshan M., Patrick Cahan, Alex K. Shalek, Rahul Satija, Ajay DaleyKeyser, Hu Li, Jin Zhang, et al. 2014. “Deconstructing Transcriptional Heterogeneity in Pluripotent Stem Cells.” *Nature* 516 (7529): 56–61.

Leitch, Harry G., Kirsten R. McEwen, Aleksandra Turp, Vesela Encheva, Tom Carroll, Nils Grabole, William Mansfield, et al. 2013. “Naive Pluripotency Is Associated with Global DNA Hypomethylation.” *Nature Structural & Molecular Biology* 20 (3): 311–16.

Marks, Hendrik, Tüzer Kalkan, Roberta Menafra, Sergey Denissov, Kenneth Jones, Helmut Hofemeister, Jennifer Nichols, et al. 2012. “The Transcriptional and Epigenomic Foundations of Ground State Pluripotency.” *Cell* 149 (3): 590–604.

Marruecos, Laura, Joan Bertran, Daniel Álvarez-Villanueva, María Carmen Mulero, Yolanda Guillén, Luis G. Palma, Martin Floor, et al. 2021. “Dynamic Chromatin Association of IκBα Is Regulated by Acetylation and Cleavage of Histone H4.” *EMBO Reports* 22 (8): e52649.

Marruecos, Laura, Joan Bertran, Yolanda Guillén, Jéssica González, Raquel Batlle, Erika López-Arribillaga, Marta Garrido, et al. 2020. “IκBα Deficiency Imposes a Fetal Phenotype to Intestinal Stem Cells.” *EMBO Reports* 21 (6): e49708.

Martinez Arias, Alfonso, and Joshua M. Brickman. 2011. “Gene Expression Heterogeneities in Embryonic Stem Cell Populations: Origin and Function.” *Current Opinion in Cell Biology* 23 (6): 650–56.

Mulero, María Carmen, Dolors Ferres-Marco, Abul Islam, Pol Margalef, Matteo Pecoraro, Agustí Toll, Nils Drechsel, et al. 2013. “Chromatin-Bound IκBα Regulates a Subset of Polycomb Target Genes in Differentiation and Cancer.” *Cancer Cell* 24 (2): 151–66.

Singer, Zakary S., John Yong, Julia Tischler, Jamie A. Hackett, Alphan Altinok, M. Azim Surani, Long Cai, and Michael B. Elowitz. 2014. “Dynamic Heterogeneity and DNA Methylation in Embryonic Stem Cells.” *Molecular Cell* 55 (2): 319–31.

Thambyrajah, Roshana, Zaki Fadlullah, Martin Proffitt, Wen Hao Neo, Yolanda Guillén, Marta Casado-Pelaez, Patricia Herrero-Molinero, et al. 2022. “IκBα Controls Dormancy Induction in Hematopoietic Stem Cell Development via Retinoic Acid.” *bioRxiv*. https://doi.org/10.1101/2022.11.17.516971.

Tian, Tian V., Bruno Di Stefano, Grégoire Stik, Maria Vila-Casadesús, José Luis Sardina, Enrique Vidal, Alessandro Dasti, et al. 2019. “Whsc1 Links Pluripotency Exit with Mesendoderm Specification.” *Nature Cell Biology* 21 (7): 824–34.

Torres, Josema, and Fiona M. Watt. 2008. “Nanog Maintains Pluripotency of Mouse Embryonic Stem Cells by Inhibiting NFkappaB and Cooperating with Stat3.” *Nature Cell Biology* 10 (2): 194–201.

Wang, Yangming, Rostislav Medvid, Collin Melton, Rudolf Jaenisch, and Robert Blelloch. 2007. “DGCR8 Is Essential for microRNA Biogenesis and Silencing of Embryonic Stem Cell Self-Renewal.” *Nature Genetics* 39 (3): 380–85.

Ying, Qi-Long, Jason Wray, Jennifer Nichols, Laura Batlle-Morera, Bradley Doble, James Woodgett, Philip Cohen, and Austin Smith. 2008. “The Ground State of Embryonic Stem Cell Self-Renewal.” *Nature* 453 (7194): 519–23.

857 Zhang, Qian, Michael J. Lenardo, and David Baltimore. 2017. “30 Years of NF-κB: A
858 Blossoming of Relevance to Human Pathobiology.” *Cell* 168 (1-2): 37–57.
859 Zhou, Wanding, Toshinori Hinoue, Bret Barnes, Owen Mitchell, Waleed Iqbal, Sol Moe Lee,
860 Kelly K. Foy, et al. 2022. “DNA Methylation Dynamics and Dysregulation Delineated by
861 High-Throughput Profiling in the Mouse.” *Cell Genomics* 2 (7).
862 https://doi.org/10.1016/j.xgen.2022.100144.

Figure 1

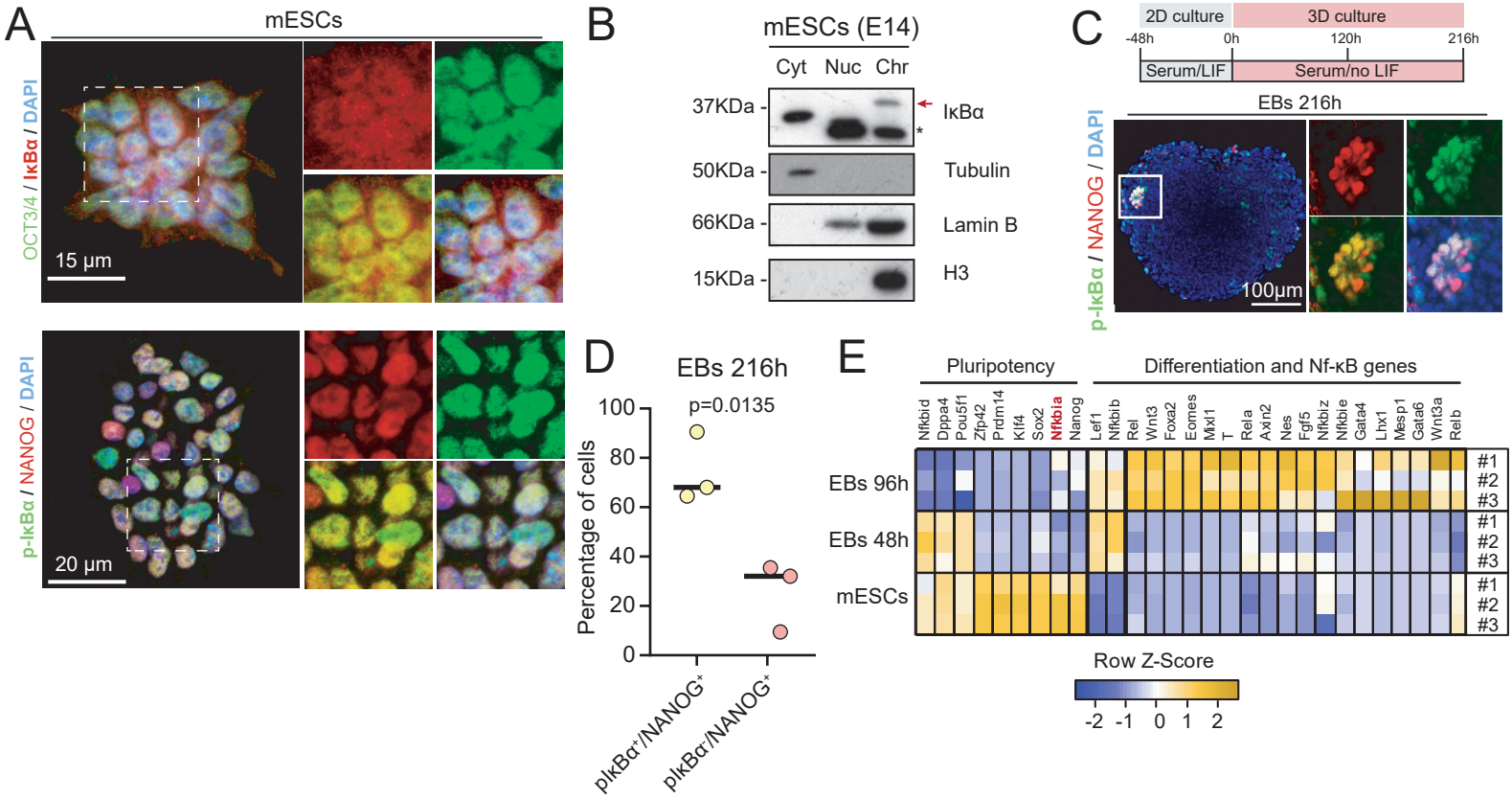
A
mESCs
OCT3/4 / IκBα / DAPI
15 µm
p-IκBα / NANOG / DAPI
20 µm
B
mESCs (E14)
Cyt Nuc Chr
37KDa -
50KDa -
66KDa -
15KDa -
IκBα
Tubulin
Lamin B
H3
C
2D culture
3D culture
-48h
0h
120h
216h
Serum/LIF
Serum/no LIF
EBs 216h
p-IκBα / NANOG / DAPI
100µm
D
EBs 216h
p=0.0135
Percentage of cells
100
80
60
40
20
0
pIκBα+/NANOG+
pIκBα-/NANOG+
E
Pluripotency
Differentiation and Nf-κB genes
Nfkbid
Dppa4
Pou5f1
Zfp42
Prdm14
Klf4
Sox2
Nfkbia
Nanog
Lef1
Nfkbib
Rel
Wnt3
Foxa2
Eomes
Mxl1
T
Rela
Axin2
Nes
Fgf5
Nfkbiz
Nfkbie
Gata4
Lhx1
Mesp1
Gata6
Wnt3a
Relb
EBs 96h
EBs 48h
mESCs
#1
#2
#3
Row Z-Score
-2 -1 0 1 2

Figure 2

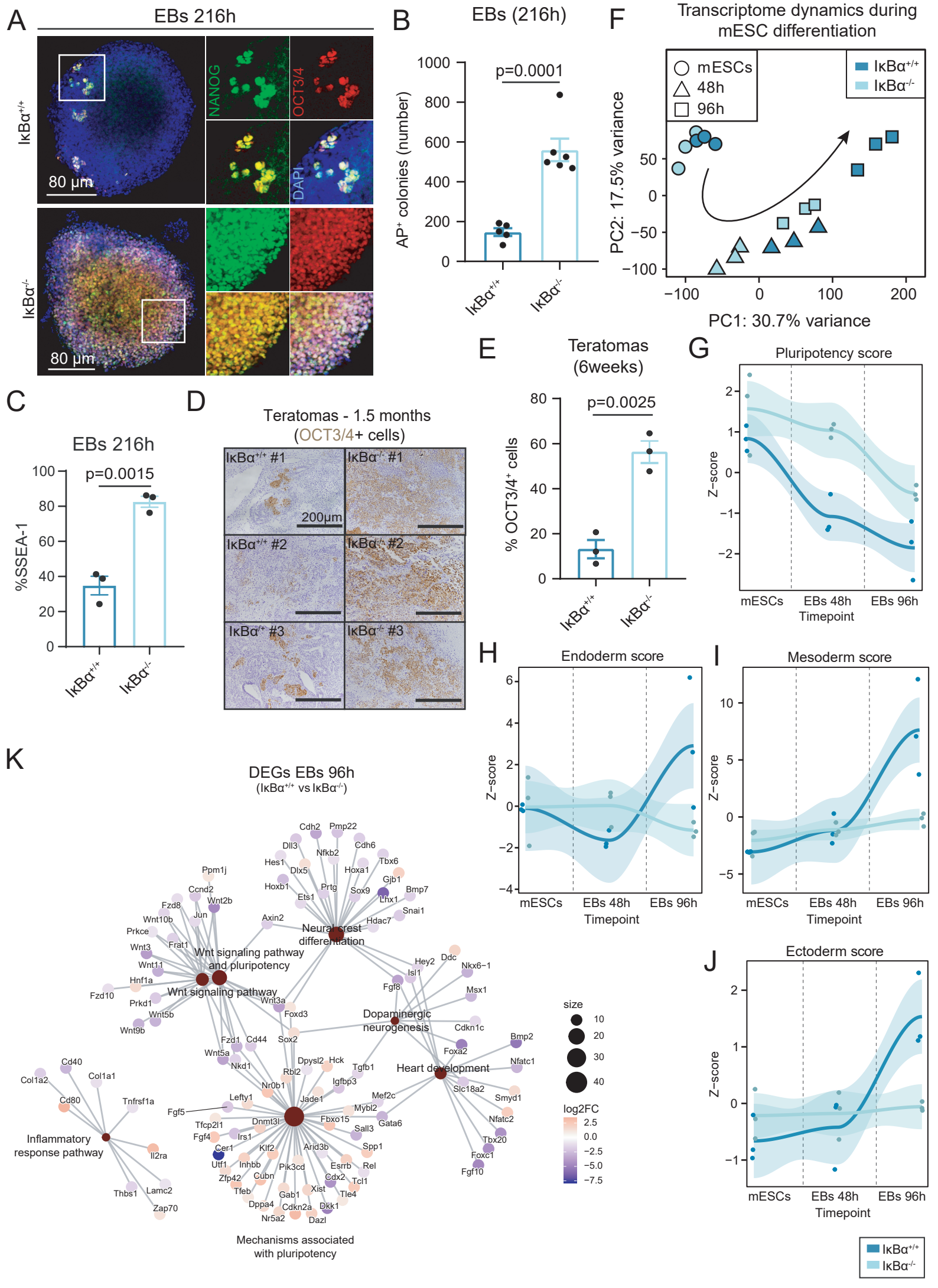
A
EBs 216h
IκBα+/+
IκBα-/-
NANOG
OCT3/4
DAPI
80 µm
B
EBs (216h)
p=0.0001
AP+ colonies (number)
C
EBs 216h
p=0.0015
%SSEA-1
D
Teratomas - 1.5 months
(OCT3/4+ cells)
IκBα+/+ #1
IκBα-/- #1
IκBα+/+ #2
IκBα-/- #2
IκBα+/+ #3
IκBα-/- #3
200µm
E
Teratomas
(6weeks)
p=0.0025
% OCT3/4+ cells
F
Transcriptome dynamics during
mESC differentiation
mESCs
48h
96h
PC2: 17.5% variance
PC1: 30.7% variance
G
Pluripotency score
Z-score
mESCs
EBs 48h
EBs 96h
Timepoint
H
Endoderm score
I
Mesoderm score
J
Ectoderm score
K
DEGs EBs 96h
(IκBα+/+ vs IκBα-/-)
Neural crest differentiation
Wnt signaling pathway and pluripotency
Wnt signaling pathway
Dopaminergic neurogenesis
Heart development
Inflammatory response pathway
Mechanisms associated with pluripotency
size
log2FC

Figure 3

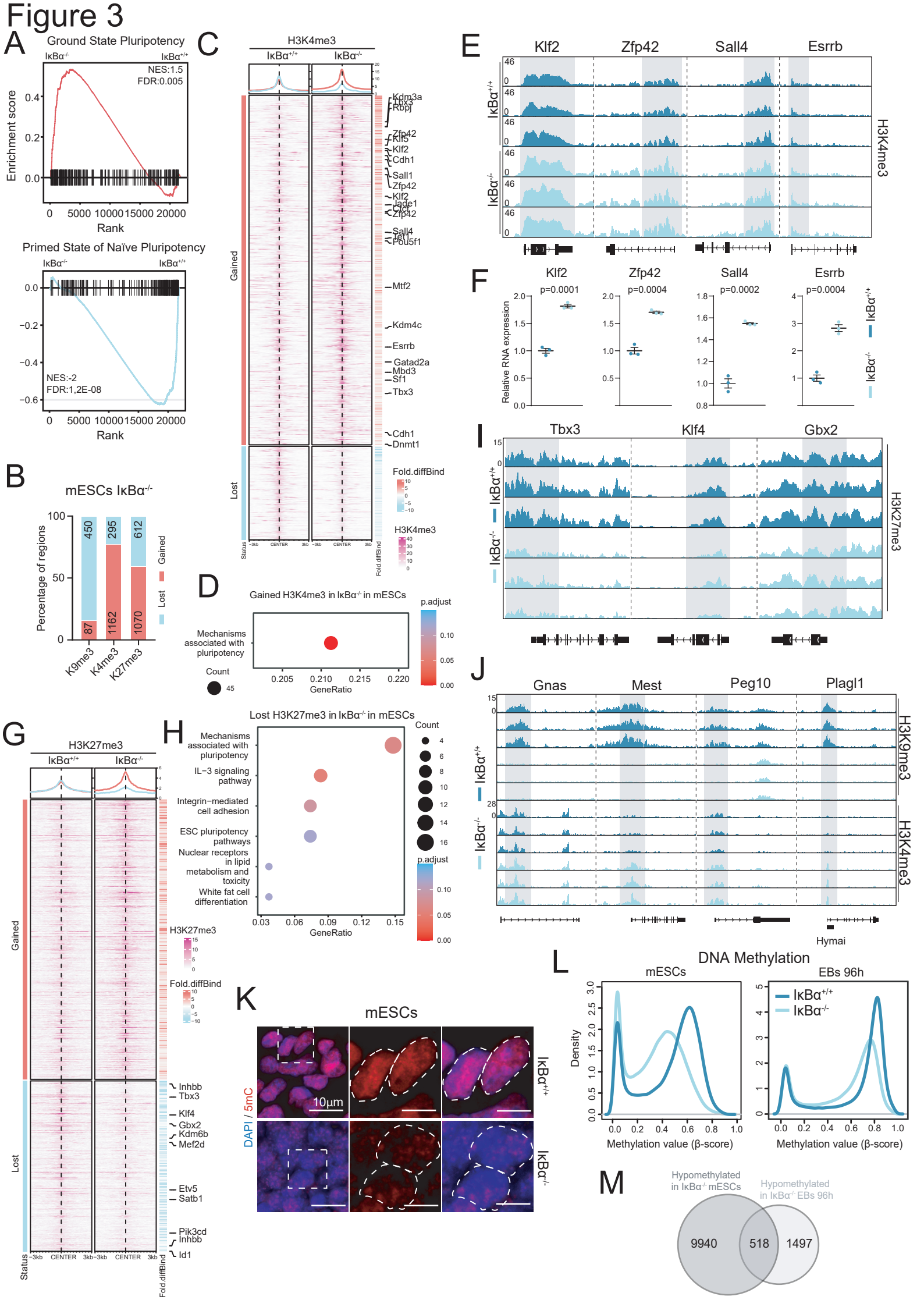
A
Ground State Pluripotency
IκBα-/-
IκBα+/+
NES:1.5
FDR:0.005
Enrichment score
Rank
Primed State of Naïve Pluripotency
NES:-2
FDR:1,2E-08
B
mESCs IκBα-/-
Percentage of regions
Gained
Lost
K9me3
K4me3
K27me3
C
H3K4me3
Gained
Lost
Fold.diffBind
D
Gained H3K4me3 in IκBα-/- in mESCs
Mechanisms associated with pluripotency
Count
p.adjust
GeneRatio
E
Klf2
Zfp42
Sall4
Esrrb
H3K4me3
F
Relative RNA expression
p=0.0001
p=0.0004
p=0.0002
p=0.0004
I
Tbx3
Klf4
Gbx2
H3K27me3
J
Gnas
Mest
Peg10
Plagl1
H3K9me3
H3K4me3
Hymai
G
H3K27me3
H
Lost H3K27me3 in IκBα-/- in mESCs
Mechanisms associated with pluripotency
IL-3 signaling pathway
Integrin-mediated cell adhesion
ESC pluripotency pathways
Nuclear receptors in lipid metabolism and toxicity
White fat cell differentiation
K
mESCs
DAPI / 5mC
10μm
L
DNA Methylation
mESCs
EBs 96h
Density
Methylation value (β-score)
M
Hypomethylated in IκBα-/- mESCs
Hypomethylated in IκBα-/- EBs 96h
9940
518
1497

Figure 4

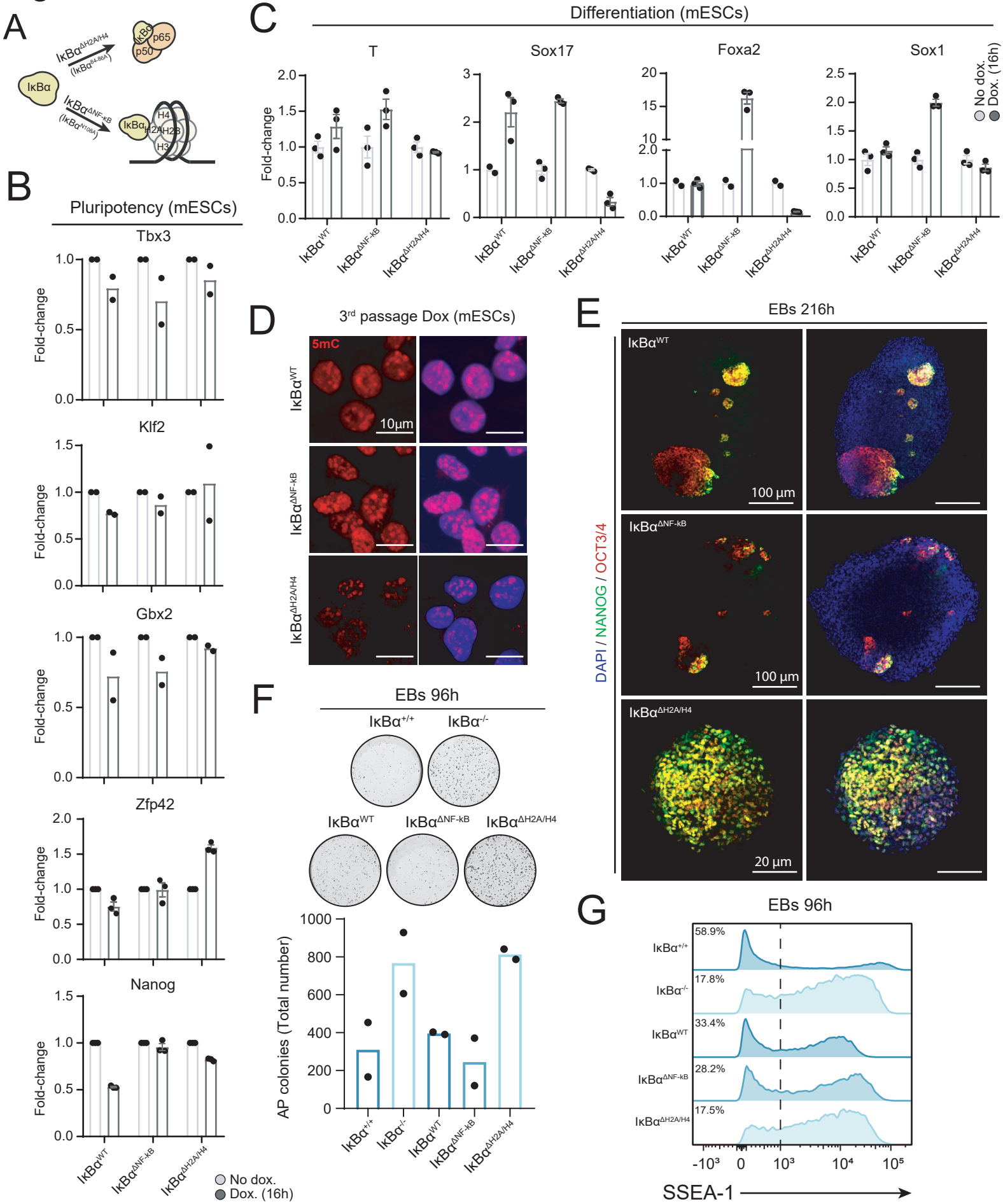
A
IκBα
IκBα^ΔH2A/H4
(IκBα^84-86A)
IκBα
p65
p50
IκBα^ΔNF-κB
(IκBα^M108A)
IκBα
H4
H2A/H2B
H3
B
Pluripotency (mESCs)
Tbx3
Klf2
Gbx2
Zfp42
Nanog
Fold-change
IκBα^WT
IκBα^ΔNF-κB
IκBα^ΔH2A/H4
No dox.
Dox. (16h)
C
Differentiation (mESCs)
T
Sox17
Foxa2
Sox1
Fold-change
IκBα^WT
IκBα^ΔNF-κB
IκBα^ΔH2A/H4
No dox.
Dox. (16h)
D
3rd passage Dox (mESCs)
5mC
10µm
IκBα^WT
IκBα^ΔNF-κB
IκBα^ΔH2A/H4
E
EBs 216h
IκBα^WT
IκBα^ΔNF-κB
IκBα^ΔH2A/H4
100 µm
100 µm
20 µm
DAPI / NANOG / OCT3/4
F
EBs 96h
IκBα^+/+
IκBα^-/-
IκBα^WT
IκBα^ΔNF-κB
IκBα^ΔH2A/H4
AP colonies (Total number)
G
EBs 96h
IκBα^+/+
IκBα^-/-
IκBα^WT
IκBα^ΔNF-κB
IκBα^ΔH2A/H4
58.9%
17.8%
33.4%
28.2%
17.5%
SSEA-1